

# Skyrmion dynamics in a chiral magnet driven by periodically varying spin currents

Rui Zhu\* and Yin-Yan Zhang

*Department of Physics, South China University of Technology,  
Guangzhou 510641, People's Republic of China*

## Abstract

In this work, we investigated the spin dynamics in a slab of chiral magnets induced by an alternating (ac) spin current. Periodic trajectories of the skyrmion in real space are discovered under the ac current as a result of the competition among the Gilbert-damping-induced skyrmion Hall motion, the spin transfer torque, and the  $\beta$ -nonadiabatic torque effects. The results are obtained by numerically solving the Landau-Lifshitz-Gilbert equation and can be explained by the Thiele equation characterizing the skyrmion core motion.

PACS numbers: 75.78.-n, 72.25.-b, 71.70.-d

arXiv:1606.09326v1 [cond-mat.mes-hall] 30 Jun 2016

---

\* Corresponding author. Electronic address: rzhu@scut.edu.cn

## I. INTRODUCTION

The skyrmion (SkM) spin texture is a kind of topologically-nontrivial magnetic vortex formed most typically in the bulk chiral magnets (CMs) and magnetic thin films<sup>1-3</sup>. In CMs it is believed that the spin-orbit coupling induced Dzyaloshinskii-Moriya (DM) interaction governs the spin spiraling mechanisms<sup>1</sup>. Recently the magnetic SkM structure attracts intensive focus, both in the fundamental theoretic aspect and in its potential application in the information technology. In the magnetic SkM state the emergent electrodynamic effect originates from its nontrivial spin topology and gives rise to the topological Hall effect and a remarkable current-driven spin transfer torque effect<sup>1,4-10</sup>. The so-called skyrmionics makes use of the SkM as a memory unit favored by its topologically protected long lifetime and ultralow driving current, which is five or six orders smaller than that to drive a magnetic domain wall<sup>1,11</sup>.

Although the current-driven spin dynamics in the CMs with DM interaction has been intensively studied recently, less work of an alternating current (ac) driven skyrmion dynamics was reported. The SkM-motion-induced ac current generation has been predicted, which shares the reversed effect of our consideration<sup>12</sup>. In this work, we investigated the ac-spin-current driven skyrmion dynamics with the DM interaction, Gilbert damping<sup>13</sup>, adiabatic and nonadiabatic spin torques, and different current profiles taken into account. Our proposition is inspired by the following several aspects. Firstly, it is both theoretically and technically interesting to know the behavior of a SkM when an external ac current is applied. Secondly, a high-speed low-power modulation of a SkM is favorable for potential memory processing. Lastly but not least, we noticed the mathematical significance of the solution of the Landau-Lifshitz-Gilbert (LLG) equation of a collinear magnet with periodically varying spin-currents applied, in which chaos is observed.

The topological property of a spin texture can be described by the surface integral of the solid angle of the unitary spin-field vector  $\mathbf{n}(\mathbf{r})$ . The SkM number is so defined as  $S = \frac{1}{4\pi} \int \mathbf{n} \cdot \left( \frac{\partial \mathbf{n}}{\partial x} \times \frac{\partial \mathbf{n}}{\partial y} \right) d^2 \mathbf{r}$  counting how many times the spin field wraps the unit sphere. More specific topological properties of a SkM can be considered by analyzing its radial and whirling symmetric pattern<sup>1</sup>. As a result of topological protection, the SkM cannot be generated from a topologically trivial magnetic state such as a ferromagnet or a helimagnet by variation without a topologically nontrivial force such as a spatially uniform external spin

current and vice versa. It is predicted by simulation that the skyrmion can be generated from a quasi-ferromagnetic and helimagnetic state by external Lorentzian and radial spin current<sup>8</sup>. The local current flowing from the scanning tunneling microscope to generate the SkM in experiment can be approximated by a radial spin current, which imbues nontrivial topology into the helimagnet<sup>7</sup>. Also an artificial magnetic SkM can be tailored by an external magnetic field with nontrivial geometric distribution<sup>14</sup>. When the boundary geometry of the material is tailored such as by a notch in a long plate, a SkM can be generated by a collinear spin current<sup>9</sup>. In this case, the nontrivial constriction topology contributes to the formation of the SkM. The uniform current can move and rotate a SkM without changing its topology<sup>11,15</sup>. In this work we will show that these topological behaviors of the SkM structure are retained in the spin dynamics driving by an ac spin current.

Almost all kinds of ferromagnetic and vortex spin dynamics can be described by the LLG equation. The behavior of the LLG equation is of importance in both the physical and mathematical sciences<sup>16</sup>. It has been shown by previous works that the spin torque effect driven by a periodic varying spin current can be described as well by the LLG equation with the original time-independent current replaced by the time-dependent current in the spin torque term<sup>16,17</sup>. Although chaotic behaviors are predicted in the spatially-uniform ac spin-current driven collinear ferromagnetic spin structure<sup>16,17</sup>, which is well described by the single-spin LLG equation, no similar phenomenon is reported in a spatially-nonuniform spin lattice, the latter of which can be attributed to the relaxation processes of the inter-site scattering. Even if some sort of chaotic behavior occurs after a long time of evolution, it is workable to restore the original state by applying a magnetic field after some time. The influence of it on the skyrmionic exploitation is not large. In this work, we use a matrix-based fourth-order Runge-Kutta method to solve the LLG equation with both the adiabatic and nonadiabatic spin torque taken into account. Analytical solution of the generalized Thiele equation<sup>1,9,15</sup> reproduces our numerical results.

## II. THEORETIC FORMALISM

We consider a thin slab of CM modulated by a constant magnetic field and an ac spin current. The strong DM interaction makes the material a SkM-host. In the continuum approximation, the Hamiltonian of the localized magnetic spin in a CM can be described

as<sup>1,8,9</sup>

$$\begin{aligned}
H = & -J \sum_{\mathbf{r}} \mathbf{M}_{\mathbf{r}} \cdot (\mathbf{M}_{\mathbf{r}+\mathbf{e}_x} + \mathbf{M}_{\mathbf{r}+\mathbf{e}_y}) \\
& -D \sum_{\mathbf{r}} (\mathbf{M}_{\mathbf{r}} \times \mathbf{M}_{\mathbf{r}+\mathbf{e}_x} \cdot \mathbf{e}_x + \mathbf{M}_{\mathbf{r}} \times \mathbf{M}_{\mathbf{r}+\mathbf{e}_y} \cdot \mathbf{e}_y) \\
& -\mathbf{B} \cdot \sum_{\mathbf{r}} \mathbf{M}_{\mathbf{r}},
\end{aligned} \tag{1}$$

with  $J$  and  $D$  the ferromagnetic and DM exchange energies, respectively. The dimensionless local magnetic moments  $\mathbf{M}_{\mathbf{r}}$  are defined as  $\mathbf{M}_{\mathbf{r}} \equiv -\mathbf{S}_{\mathbf{r}}/\hbar$ , where  $\mathbf{S}_{\mathbf{r}}$  is the local spin at  $\mathbf{r}$  and  $\hbar$  is the plank constant divided by  $2\pi$ . We assume that the length of the vector  $|\mathbf{M}_{\mathbf{r}}| = M$  is fixed, therefore  $\mathbf{M}_{\mathbf{r}} = M\mathbf{n}(\mathbf{r})$  with  $\mathbf{n}(\mathbf{r})$  the unitary spin field vector. The unit-cell dimension is taken to be unity. An external magnetic field  $\mathbf{B}$  is applied perpendicular to the slab plane to stabilize the SkM configuration. The Bohr magneton  $\mu_B$  is absorbed into  $\mathbf{B}$  to have it in the unit of energy. The typical DM interaction  $D = 0.18J$  is used throughout this work<sup>9</sup>. This DM exchange strength corresponds to the critical magnetic fields  $B_{c1} = 0.0075J$  between the helical and SkM-crystal phases and  $B_{c2} = 0.0252J$  between the SkM-crystal and ferromagnetic phases, respectively. We adopt  $\mathbf{B} = (0, 0, 0.01J)$  in our numerical considerations with  $J = 1$  meV.

The extended form of the LLG equation that takes into account the DM interaction and the adiabatic and nonadiabatic spin torque effect can be expressed in the following formula<sup>1,8,9,18</sup>

$$\begin{aligned}
\frac{d\mathbf{M}_{\mathbf{r}}}{dt} = & -\gamma \mathbf{M}_{\mathbf{r}} \times \mathbf{B}_{\mathbf{r}}^{\text{eff}} + \frac{\alpha}{M} \mathbf{M}_{\mathbf{r}} \times \frac{d\mathbf{M}_{\mathbf{r}}}{dt} + \frac{pa^3}{2eM} [\mathbf{j}(\mathbf{r}, t) \cdot \nabla] \mathbf{M}_{\mathbf{r}} \\
& - \frac{pa^3\beta}{2eM^2} \{ \mathbf{M}_{\mathbf{r}} \times [\mathbf{j}(\mathbf{r}, t) \cdot \nabla] \mathbf{M}_{\mathbf{r}} \}.
\end{aligned} \tag{2}$$

By assuming that the energy of a magnet with the local magnetization  $\mathbf{M}_{\mathbf{r}}$  in a spatially varying magnetic field  $\mathbf{B}_{\mathbf{r}}^{\text{eff}}$  has the form of  $H = -\gamma\hbar \sum_{\mathbf{r}} \mathbf{M}_{\mathbf{r}} \cdot \mathbf{B}_{\mathbf{r}}^{\text{eff}}$ , we have

$$\mathbf{B}_{\mathbf{r}}^{\text{eff}} = -\frac{1}{\hbar\gamma} \frac{\partial H}{\partial \mathbf{M}_{\mathbf{r}}}, \tag{3}$$

and therefore the first term in the right hand side of Eq. (2) is

$$\begin{aligned}
-\gamma \mathbf{M}_{\mathbf{r}} \times \mathbf{B}_{\mathbf{r}}^{\text{eff}} = & -\frac{J}{\hbar} \mathbf{M}_{\mathbf{r}} \times (\mathbf{M}_{\mathbf{r}+\mathbf{e}_x} + \mathbf{M}_{\mathbf{r}+\mathbf{e}_y} + \mathbf{M}_{\mathbf{r}-\mathbf{e}_x} + \mathbf{M}_{\mathbf{r}-\mathbf{e}_y}) - \frac{1}{\hbar} (\mathbf{M}_{\mathbf{r}} \times \mathbf{B}) \\
& - \frac{D}{\hbar} \mathbf{M}_{\mathbf{r}} \times \left[ \begin{aligned} & (\mathbf{M}_{\mathbf{r}-\mathbf{e}_y,z} - \mathbf{M}_{\mathbf{r}+\mathbf{e}_y,z}) \mathbf{e}_x + (\mathbf{M}_{\mathbf{r}+\mathbf{e}_x,z} - \mathbf{M}_{\mathbf{r}-\mathbf{e}_x,z}) \mathbf{e}_y \\ & + (\mathbf{M}_{\mathbf{r}+\mathbf{e}_y,x} - \mathbf{M}_{\mathbf{r}+\mathbf{e}_x,y} - \mathbf{M}_{\mathbf{r}-\mathbf{e}_y,x} + \mathbf{M}_{\mathbf{r}-\mathbf{e}_x,y}) \mathbf{e}_z \end{aligned} \right].
\end{aligned} \tag{4}$$

The second to the last terms of Eq. (2) sequentially corresponds to the effect of the Gilbert damping, the time-dependent spin current  $\mathbf{j}(t) = \mathbf{j}_e \sin(\omega t)$ -induced adiabatic and nonadiabatic spin torques, respectively.  $p$  measures the polarization of the conduction electrons,  $e$  is

the positive electron charge, and  $a$  is the average in-plane lattice constant of the CM. In our considerations the frequency of the ac spin current  $\omega$  is small enough in comparison of the magnetization evolution rate. Therefore, the spin torques can be satisfactorily described by using the time-dependent current in the standard torque expression, which has been justified by previous studies<sup>16,17</sup>. Here, the unit of time is set to be  $t_0 = \hbar/J \approx 6.6 \times 10^{-13}$  s. A phenomenologically expected value of  $\alpha = 0.1$  is used in afterwards numerical considerations.

By looking deep into Eqs. (2) and (4), we can make some predictions of the behavior of the local magnetization. We know that the effect of the magnetic field together with the Gilbert term is to precess the magnetic spin into the direction of the external field. The first term in the right hand side of Eq. (4) is that the effective magnetic field is in the direction of neighboring spins. Therefore the evolution tends to form a ferromagnet. This contributes to the velocity of the magnetization is in the direction of  $\mathbf{M}_{\mathbf{r}} \times \mathbf{M}_{\mathbf{r}'}$ , which is precession of one around the other. The effective field in the DM term in Eq. (4) is  $-\nabla \times \mathbf{M}_{\mathbf{r}}$  with unitary lattice constants. The integral counterpart of the curl is  $\oint \mathbf{M}_{\mathbf{r}'} \cdot d\mathbf{l}$ . When the neighboring spins form a ring, the energy is the lowest, hence generating a spiraling force to the CM. It helps our understanding if we analogize all the other terms in the right hand side of Eq. (2) to the effect of a magnetic field. The local “magnetic field” of the phenomenological Gilbert damping force is proportional to  $-d\mathbf{M}_{\mathbf{r}}/dt$  in the standard linear-response damping form, proportional to the velocity and pointing oppositely to it. While the local spin is precessing, the direction of  $\mathbf{M}_{\mathbf{r}} \times d\mathbf{M}_{\mathbf{r}}/dt$  points to the precession axis of  $\mathbf{M}_{\mathbf{r}}$  adding a force swaying to that axis. The last two terms are the effect of the current-induced spin torques. For convenience of interpretation, we discuss the case that  $\mathbf{j}(\mathbf{r}, t)$  is spatially-uniform and along the  $x$ -direction. Then  $[\mathbf{j}(\mathbf{r}, t) \cdot \nabla] \mathbf{M}_{\mathbf{r}} = j_x(t) \partial \mathbf{M}_{\mathbf{r}} / \partial x$ . In the case of the adiabatic torque, this term adds a velocity to  $\mathbf{M}_{\mathbf{r}}$  making it sway to the direction of  $\mathbf{M}_{\mathbf{r}+\mathbf{e}_x}$ , and  $\mathbf{M}_{\mathbf{r}+\mathbf{e}_x}$  to  $\mathbf{M}_{\mathbf{r}+2\mathbf{e}_x}$ , and etc. if  $j_x(t)$  is positive. Therefore, the complete spin texture moves along the direction of the external spin current like a relay race no matter it is a SkM or a domain wall. In a periodic magnetic structure such as a ferromagnet and a helimagnet the “relay race” goes back to itself and hence no spin structure movement occurs. Following this physical picture, the local “magnetic field” of the nonadiabatic spin torque is along the direction of  $j_x(t) \partial \mathbf{M}_{\mathbf{r}} / \partial x$ . It exerts a velocity perpendicular to that originates from the adiabatic spin torque. Its result is the motion of the spin texture in the direction perpendicular to the spin current. We have already analyzed the mechanisms of the LLG equation term by term.

However, they affects the system collaboratively. While the adiabatic spin torque moves the SkM along the spin current, the Gilbert damping force contributes a velocity in the direction of  $\mathbf{M}_r \times d\mathbf{M}_r/dt$  and therefore the effect is a transverse motion of the SkM, which is the so-called Hall-like motion<sup>8</sup>. Also it is noticeable that the transverse velocity contributed from the Gilbert damping and the nonadiabatic spin torque is opposite to each other. In real situations, both  $\alpha$  and  $\beta$  are much less than 1. The adiabatic spin torque makes the main contribution to the motion of the SkM. And when the two transverse force is equal, the motion of the SkM is straightly along the direction of the spin current. Therefore, periodic trajectories of the SkM in real space can be predicted influenced by a spatially uniform ac spin current.

The previous discussions are well expressed in the Thiele equation describing the motion of the center of mass of a SkM as<sup>1,9,15,19</sup>.

$$\mathbf{G} \times [-\mathbf{j}(t) - \mathbf{v}_d] + \kappa [-\beta\mathbf{j}(t) - \alpha\mathbf{v}_d] - \nabla U(\mathbf{r}) = \mathbf{0}, \quad (5)$$

where  $\mathbf{v}_d = d\mathbf{R}/dt = (\dot{X}, \dot{Y})$  with  $\mathbf{R} = (X, Y)$  the center of mass coordinates,  $\kappa$  is a dimensionless constant of the order of unity, and  $\mathbf{G} = 2\pi S\mathbf{e}_z$  is the gyrovector with  $\mathbf{e}_z$  in the direction perpendicular to the CM plane. The minus sign before  $\mathbf{j}(t)$  is because of that the direction of the motion of conduction electrons is opposite to that of the current. In our considerations, periodic boundary conditions are used to justify an infinite two-dimensional model. The applied magnetic field is spatially uniform and the impurity effect is neglected. Therefore  $\nabla U \approx 0$ . The analytical result of Eq. (5) assuming  $S = -1$  and  $\mathbf{j}(t) = j_e \sin(\omega t) \mathbf{e}_x$  can be obtained as

$$\begin{cases} X = \frac{\alpha\beta\kappa^2 + 4\pi^2}{(\alpha^2\kappa^2 + 4\pi^2)\omega} j_e \cos(\omega t), \\ Y = \frac{2\pi\kappa(\beta - \alpha)}{(\alpha^2\kappa^2 + 4\pi^2)\omega} j_e \cos(\omega t), \end{cases} \quad (6)$$

which agrees with the numerical results demonstrated in the following section. Because the SkM vortex moves in the relay flashing under the effect of the spin torque shown by the LLG equation, there is a  $\pi/2$  phase lag between its core motion and the sinusoidally varying spin current.

### III. NUMERICAL RESULTS AND INTERPRETATIONS

By multiplying  $\tilde{\alpha}^{-1}$  with

$$\tilde{\alpha} = 1 - \alpha \begin{bmatrix} 0 & -(\mathbf{M}_{\mathbf{r}})_z & (\mathbf{M}_{\mathbf{r}})_y \\ (\mathbf{M}_{\mathbf{r}})_z & 0 & -(\mathbf{M}_{\mathbf{r}})_x \\ -(\mathbf{M}_{\mathbf{r}})_y & (\mathbf{M}_{\mathbf{r}})_x & 0 \end{bmatrix}, \quad (7)$$

from the left to Eq. (2), the matrix-based Runge-Kutta method is developed. In Figs. 1 to 3, numerical results of our simulations are given. We set  $M = 1$ ,  $p = 0.5$ , and  $a = 4 \text{ \AA}$ . The integral step  $h = 0.1t_0$  is used and its convergence is justified by comparison with the results of  $h = 0.01t_0$ . With  $D = 0.18J$ , the natural helimagnet wavevector  $Q = 2\pi/\lambda = D/J$  with the diameter of the SkM  $\lambda = D/J \approx 35$  in the unit of  $a$ . A  $30 \times 30$  square lattice is considered which approximately sustains a single SkM. Periodic boundary condition is used to allow the considered patch to fit into an infinite plane. While part of the SkM moves out of the slab, complementary part enters from the outside as the natural ground state of a CM is the SkM crystal. We use the theoretically perfect SkM profile  $\mathbf{n}(\mathbf{r}) = [\cos \Phi(\varphi) \sin \Theta(r), \sin \Phi(\varphi) \sin \Theta(r), \cos \Theta(r)]$  with  $\Theta(r) = \pi(1 - r/\lambda)$  and  $\Phi(\varphi) = \varphi$  in the polar coordinates as the initial state and it would change into a natural SkM in less than one current period. The SkM number for this state  $S = -1$ . The spatially-uniform ac spin current is applied in the  $x$ -direction as  $\mathbf{j}(t) = j_e \sin(\omega t) \mathbf{e}_x$  within the CM plane.

Variation of the SkM number in time driven by the ac spin current is shown in Fig. 1. It can be seen that cosinusoidal variation of  $S$  originates from the sinusoidal  $\mathbf{j}(t)$  with exactly the same period. Fig. 2 shows the snapshots of the spin profile at the bottoms and peaks of the cosinusoidal variation of  $S$  and Fig. 3 shows the trajectories of the center of the SkM. The SkM number is a demonstration of the motion pattern of the SkM. While the SkM moves to one side of the CM slab, only part of a SkM is within the view and hence the SkM number is reduced. Previous authors have found that the velocity of the SkM increases linearly with the increase of the current amplitude and that the dynamical threshold current to move a SkM is in the same order of that needed for a domain wall<sup>1</sup>. Here we have reobtained the two points. It can be seen in Fig. 1(a) that the peak height of the SkM number increases with the amplitude of the current density and it becomes almost invisible when  $j_e$  is as small as  $10^{10} \text{ Am}^{-2}$ . In Fig. 1(b), the evolutions of  $S$  for different ac periods are shown. The frequency of the ac current is in the order of GHz,

which is sufficiently adiabatic as the rate of the spin dynamics is in the order of  $10^{-12}$  s. We can see that the periodic pattern of  $S$  is better kept with larger amplitudes for smaller ac frequencies. It shows that the phenomenon is a good adiabatic one. Within our numerical capacity, it can be predicted that strong cosinusoidal variation can occur at MHz or smaller ac frequencies, which promises experimental realization.

The variation of  $S$  is the result of the motion of the SkM. The periodic translation of SkM is the result of the combined effect of the spin torques and Gilbert-damping-induced Hall-like effect. As shown in Fig. 2, in spite of its motion, the topological properties of the SkM are conserved because the initial SkM state and the natural SkM ground state share similar topology and no topology-breaking source such as an in-plane magnetic field is present. When part of the SkM moves out of the CM slab, only the remaining part contributes to the SkM number and hence  $S$  is decreased. The cosinusoidal variation of  $S$  directly reflects the oscillating trajectory of the SkM Shown in Figs. 2 and 3. We can see that the SkM changes from the initial artificial SkM state into the natural SkM state with  $S = -1$  conserved, as shown in Fig. 2(a) and (b). At the times of integer periods the SkM is at the center of the CM slab and at the times of half-integer periods the SkM moves to the left-bottom corner as shown in Fig. 2 (c) to (f).

As predicted by the Thiele equation, the trajectory of the SkM follows a cosinusoidal pattern expressed in Eq. (6). It is interesting that the trajectory of the SkM results from the competition among the Gilbert Hall effect and the adiabatic and nonadiabatic spin torque effect. The adiabatic spin hall effect exerts a force to align the spin at each site to its  $+x$ -direction neighbor while  $\mathbf{j}(t)$  is in the  $\mathbf{e}_x$  direction, which results in the motion of the spin pattern to the  $+x$  direction in a relay fashion. The Gilbert Hall effect and the nonadiabatic spin torque add a transverse velocity to the moving SkM perpendicular to its original velocity. These two forces are in opposite directions when  $\alpha$  and  $\beta$  are both positive. Therefore the transverse motion is determined by the sign and relative strength of these two effects. From Eq. (6) we can see that when  $\beta - \alpha > 0$  the SkM's  $y$ -direction motion is in a cosinusoidal form and when  $\beta - \alpha < 0$  it is in a negative cosinusoidal form. For the  $x$ -direction motion of the SkM, the direction is the same in the two cases and the magnitude is smaller for the latter because  $|4\pi^2| \gg |\alpha\beta\kappa^2|$  holds for all physical parameter settings. And physically its because the  $x$ -direction motion of the SkM is mainly determined by the adiabatic spin torque, which is the prerequisite for any motion of the SkM.



Our simulation results of the SkM trajectories for  $\beta = 0.5$  and  $-0.5$  with fixed  $\alpha = 0.1$  are shown in Fig. 3. Good agreement with the prediction by the Thiele equation is obtained. In the two cases,  $X$  evolves cosinusoidally with the initial position  $(X, Y) = (15, 15)$  at the center of the CM slab. For  $\beta = 0.5$ ,  $Y$  evolves cosinusoidally while for  $\beta = -0.5$ ,  $Y$  evolves minus-cosinusoidally. Its oscillating amplitude is larger in Fig. 3(b). Besides the oscillation, a linear velocity of the SkM can be seen. And the directions of this velocity are different in the two cases. We attribute this linear velocity to the whirling of the SkM from the artificial initial profile to the natural profile sustained by the real CM. Because at this whirling step, the Gilbert damping and the adiabatic and nonadiabatic torques are already in effect, the initial linear velocities are different in the two cases.

#### IV. CONCLUSIONS

In this work, we have investigated the dynamics of the SkM in a CM driven by periodically varying spin currents by replacing the static current in the LLG equation by an adiabatic time-dependent current. Oscillating trajectories of the SkM are found by numerical simulations, which are in good agreement with the analytical solution of the Thiele equation. In the paper, physical behaviors of the general LLG equation with the Gilbert damping and the adiabatic and nonadiabatic spin torques coexistent are elucidated. Especially, the effect of the nonadiabatic spin torque is interpreted both physically and numerically.

#### V. ACKNOWLEDGEMENTS

R.Z. would like to thank Pak Ming Hui for stimulation and encouragement of the work. This project was supported by the National Natural Science Foundation of China (No. 11004063) and the Fundamental Research Funds for the Central Universities, SCUT (No. 2014ZG0044).

- 
- <sup>1</sup> N. Nagaosa and Y. Tokura, *Nat. Nanotechnol.* **8**, 899 (2013).
  - <sup>2</sup> S. Mühlbauer, B. Binz, F. Jonietz, C. Pfleiderer, A. Rosch, A. Neubauer, R. Georgii, and P. Böni, *Science* **323**, 915 (2009).
  - <sup>3</sup> S. Heinze, K. V. Bergmann, M. Menzel, J. Brede, A. Kubetzka, R. Wiesendanger, G. Bihlmayer, and S. Blügel, *Nat. Phys.* **7**, 713 (2011).
  - <sup>4</sup> K. Hamamoto, M. Ezawa, and N. Nagaosa, *Phys. Rev. B* **92**, 115417 (2015).
  - <sup>5</sup> A. Neubauer, C. Pfleiderer, B. Binz, A. Rosch, R. Ritz, P. G. Niklowitz, and P. Böni, *Phys. Rev. Lett.* **102**, 186602 (2009).
  - <sup>6</sup> T. Schulz, R. Ritz, A. Bauer, M. Halder, M. Wagner, C. Franz, C. Pfleiderer, K. Everschor, M. Garst, and A. Rosch, *Nat. Phys.* **8**, 301 (2012).
  - <sup>7</sup> N. Romming, C. Hanneken, M. Menzel, J. E. Bickel, B. Wolter, K. V. Bergmann, A. Kubetzka, and R. Wiesendanger, *Science* **341**, 636 (2013).
  - <sup>8</sup> Y. Tchoe and J. H. Han, *Phys. Rev. B* **85**, 174416 (2012).
  - <sup>9</sup> J. Iwasaki, M. Mochizuki, and N. Nagaosa, *Nat. Nanotechnol.* **8**, 742 (2013).
  - <sup>10</sup> D.C. Ralph and M.D. Stiles, *J. Magn. Magn. Mater.* **320**, 1190 (2008).
  - <sup>11</sup> F. Jonietz, S. Mühlbauer, C. Pfleiderer, A. Neubauer, W. Münzer, A. Bauer, T. Adams, R. Georgii, P. Böni, R. A. Duine, K. Everschor, M. Garst, and A. Rosch, *Science* **330**, 1648 (2010).
  - <sup>12</sup> S.-Z. Lin, C. D. Batista, C. Reichhardt, and A. Saxena, *Phys. Rev. Lett.* **112**, 187203 (2014).
  - <sup>13</sup> K. M. D. Hals and A. Brataas, *Phys. Rev. B* **89**, 064426 (2014).
  - <sup>14</sup> J. Li, A. Tan, K.W. Moon, A. Doran, M.A. Marcus, A.T. Young, E. Arenholz, S. Ma, R.F. Yang, C. Hwang, and Z.Q. Qiu, *Nat. Commun.* **5**, 4704 (2014).
  - <sup>15</sup> K. Everschor, M. Garst, B. Binz, F. Jonietz, S. Mühlbauer, C. Pfleiderer, and A. Rosch, *Phys. Rev. B* **86**, 054432 (2012).
  - <sup>16</sup> M. Lakshmanan, *Phil. Trans. R. Soc. A* **369**, 1280 (2011).
  - <sup>17</sup> Z. Yang, S. Zhang, and Y. C. Li, *Phys. Rev. Lett.* **99**, 134101 (2007).
  - <sup>18</sup> I. M. Miron, G. Gaudin, S. Auffret, B. Rodmacq, A. Schuhl, S. Pizzini, J. Vogel, and P. Gambardella, *Nat. Mater.* **9**, 230 (2010).
  - <sup>19</sup> A. A. Thiele, *Phys. Rev. Lett.* **30**, 230 (1972).

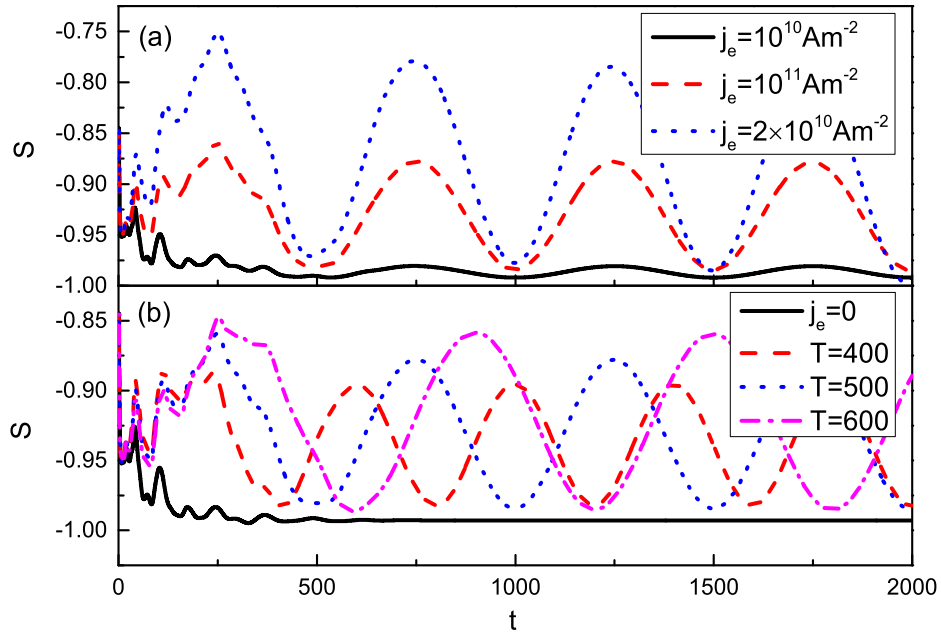


FIG. 1: Variation of the SkM number  $S$  in time (a) for different current amplitudes and (b) for different ac current frequencies. The time  $t$  and ac spin current period  $T$  are in the unit of  $t_0 \approx 6.6 \times 10^{-13}$  s. In panel (a),  $j_e = 10^{11} \text{ Am}^{-2}$ . In panel (b),  $T = 500$ .

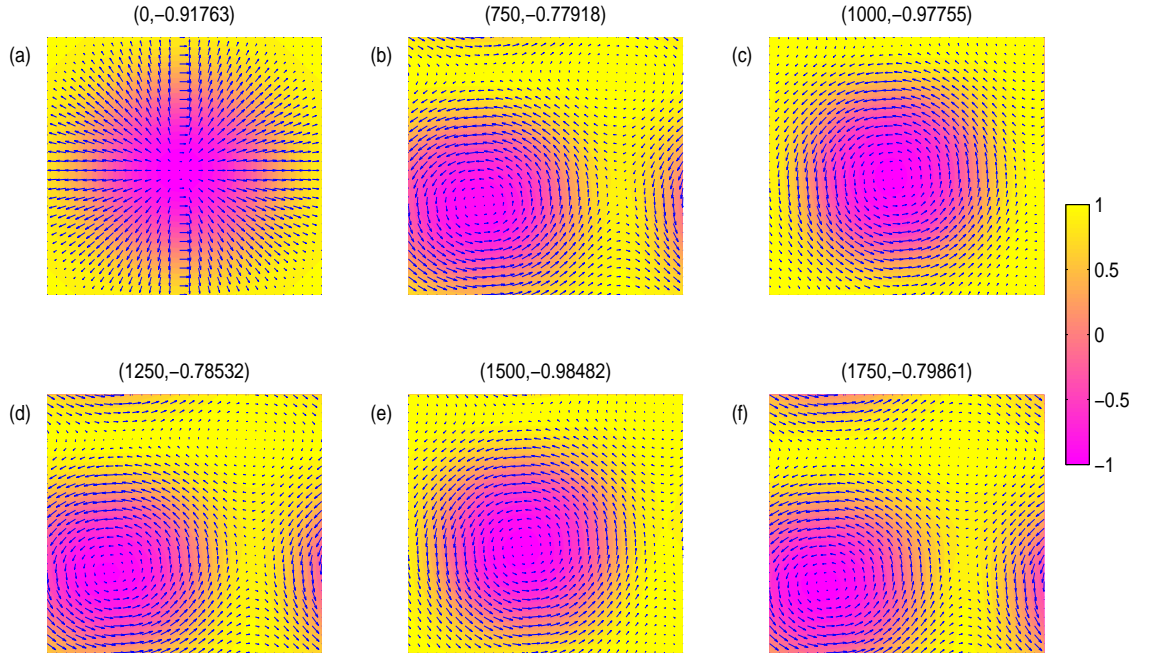


FIG. 2: Snapshots of the dynamical spin configurations at the bottoms and peaks of the SkM number shown in Fig. 1. The in-plane components of the magnetic moments are represented by arrows and their  $z$ -components are represented by the color plot. The parameters are  $j_e = 2 \times 10^{11} \text{ Am}^{-2}$ ,  $T = 500$ , and  $\beta = 0.5$ . On the top of each panel are the  $(t, S)$  values.

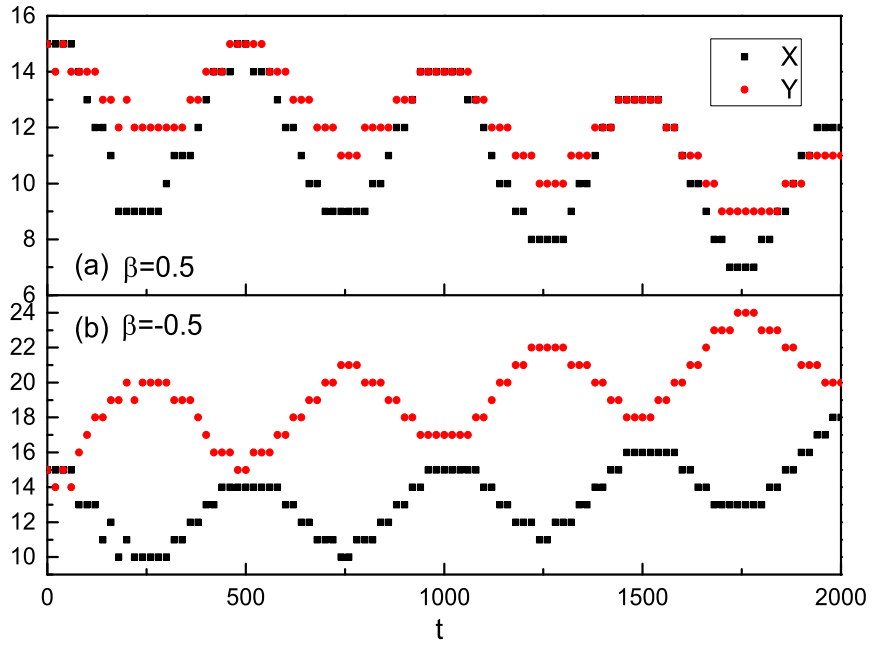


FIG. 3: Variation of the SkM center coordinates  $(X, Y)$  in time (a) for  $\beta = 0.5$  and (b) for  $\beta = -0.5$ . Other parameters are the same as Fig. 2.